Zhou et al. International Journal of Mechanical and Materials Engineering (2017) 12:6
DOI 10.1186/s40712-017-0074-6

International Journal of Mechanical and Materials Engineering

ORIGINAL ARTICLE Open Access

Surface characterization of austenitic stainless steel 304L after different grinding operations

Nian Zhou[1,2*], Ru Lin Peng[3] and Rachel Pettersson[2,4]

Abstract

Background: The austenitic stainless steel 304L is widely used as a structural material for which the finished surface has significant effect on the service performance. A study of the grinding process with regard to the quality of the ground surfaces is therefore interesting from the point of view of both industrial application and scientific research.

Method: This work investigates the influence of grinding parameters including abrasive grit size, machine power, and grinding lubrication on the surface integrity of the austenitic stainless steel 304L. The induced normal grinding force, grinding surface temperature, metal removal rate, and surface property changes have been investigated and compared.

Results and Conclusion: Using grinding, lubrication significantly enhanced the metal removal rate. Surface defects (deep grooves, smearing, adhesive chips, and indentations), a highly deformed thin surface layer up to a few microns in thickness, and high surface tensile residual stresses parallel to the grinding direction have been observed as the main damage induced by the grinding operations. Surface finish and deformation were found to be improved by using smaller abrasive grits or by using lubrication during grinding. Increasing the machine power increased surface deformation while reducing surface defects. The results obtained can provide a reference for choosing appropriate grinding parameters when machining 304L; and can also help to understand the failure mechanism of ground austenitic stainless steel components during service.

Keywords: Austenitic stainless steel 304L, Grinding, Surface characterization, Microstructure, Residual stress

Background

It is well known that the geometrical, physical, and mechanical properties of the affected surface layer from machining have significant effects on the functional performance of machined components. Service failure related to fatigue or corrosion almost always starts from the surface or near the surface of the components. Compared with mechanical polishing, surface grinding of 304L has been found to induce a higher degree of damage leading to an obvious fatigue life reduction (Poulain et al. 2013); they stated that the surface finish should be taken into account when designing components against fatigue. Stress corrosion cracking in chloride environment has been observed in 304L stainless steel in both machined and ground conditions without any externally applied loading (Acharyya et al. 2012); the high magnitude of tensile residual stresses and plastic deformation on the surface and sub-surface layers have been proposed as the main factor. A propensity for pitting to initiate at surface defect areas has been demonstrated by (Turnbull et al. 2011), and clear evidence of small embryonic cracks emerging at pits has been observed. Considering that the properties of the surface layers will be largely affected and could be controlled by the machining operation parameters, studies with various materials have been carried out to find the correlation under different manufacturing processes, such as Inconel 718 (Yao et al. 2013), Ti-6Al-4V (Guo et al. 2010), duplex stainless steel 2304 (Zhou, Peng Ling, et al. 2016).

Grinding is mainly regarded as a finishing operation, though it can also be used for bulk material removal. It is a complex cutting process with geometrically unspecified cutting edges (Dieter 1989); the grinding zone involves

* Correspondence: nzh@du.se
[1]Department of Material Science, Dalarna University, SE-79188 Falun, Sweden
[2]KTH, SE-10044 Stockholm, Sweden
Full list of author information is available at the end of the article

contact between an abrasive with a randomly structured topography and the workpiece material. The grinding process is largely influenced by the friction of the interface, the flow characteristics of the material, and the grinding speed (Kopac and Krajnik 2006). Deformation of the workpiece material is mainly introduced by the metal removal process and the rubbing contact from grinding operations (Turley and Doyle 1975). Grinding requires a high specific energy and can generate a high grinding zone temperature (Outwater and Shaw 1952). Surface properties of the components can be largely affected by the selected grinding parameters. Surface roughness, which is the foremost characteristic in surface property issues, have been reported to be significantly affected by the grinding depth and feed rate of Ti-6Al-4V (Guo et al. 2010). The extent of the deformed surface layer has been found to depend on the form of the grit as well as the rake angle for 70:30 brass (Turley and Doyle 1975). High tensile residual stresses have been observed in Inconel 718 ground surfaces by different grinding wheels (Yao et al. 2013). Compressive residual stresses have also been found in medium carbon steel when grinding using miniature monolayer electroplated CBN (cubic boron nitride) wheels (Vashista et al. 2010). The surface integrity of GH4169 was shown to be susceptible to the magnitude of cutting depth (Zeng et al. 2015). All these surface property changes due to the varied grinding parameters may largely affect the materials' performance during application. Thus, there is a need for controlled grinding processes to give a desirable surface finish to components.

However, stainless steels are commonly recognized as materials difficult to machine because of their high toughness, high work hardening rate, and low thermal conductivity. They have been characterized as 'gummy', i.e., rubbery or adhesive, during machining, showing a tendency to produce stringy chips, which degrades the surface finish and reduces tool life (Jang et al. 1996). Austenitic stainless steels are particularly challenging to machine because of their high degree of work hardening and their galling tendency (Boothroyd and Knight 2005). Grindability of four different stainless steels has been compared by (Jiang et al. 1996); high adhesion of alumina particles from alumina wheels was observed on the ground surfaces of PM 2205 and PM 2507 stainless steels. Different grinding operations have been reported to introduce different types and extent of damage in the surface and sub-surface layers of stainless steels, while some beneficial effects have also been reported. Surface burns (Zhang et al. 2012), microcracks, and micro-voids (Jiang et al. 1996) have been observed on ground stainless steel surfaces. Formation of a deformed zone near the surface with highly fragmented grain structure as well as martensitic transformation has been found for ground austenitic stainless steel 304L (Acharyya et al. 2012). Significant improvements in surface roughness and surface defects have been reported by the application of cryogenic cooling when grinding austenitic stainless steel 316 (Manimaran et al. 2014). High tensile residual stresses have shown to be introduced during grinding of austenitic stainless steel 304 (Turnbull et al. 2011), although a lower tensile residual stress was measured when grinding fluid was used (Fredj et al. 2006).

Increasing quality demands for grinding are required with respect to productivity, precision, and cost; thus, surface property issues due to grinding have become a serious cause of concern in manufacturing of stainless steel components. However, little research work has been published on the surface integrity of ground austenitic stainless steel prepared with a well-controlled grinding process. The present work aims to connect the industrial interest with scientific research by studying the grinding behavior and surface properties of austenitic stainless steel 304L. Grinding operations using different abrasive grit sizes, machine powers, and grinding lubrication, have been compared. Normal grinding force, grinding surface temperature, and metal removal rate were measured, surface properties including surface roughness and defects, cross-sectional microstructure, and surface residual stresses have been investigated. The results obtained in this study can be used as a reference to choose more effective grinding parameters for a required surface finishing when fabricating austenitic stainless steel components. The results can also help to understand the failure mechanism of austenitic stainless steels during service.

Methods

Material

The investigated material was 304L (UNS S30403) austenitic stainless steel with a chemical composition: 0.019 C, 0.32 Si, 1.55 Mn, 0.029 P, 0.001 S, 18.22 Cr, 8.11 Ni, 0.011 Nb, 0.31 Cu, 0.16 Co, 0.071 N, and balance Fe (all in wt%). During production, the as-received material had been solution annealed at 1100 °C followed by forced air cooling and water quenching. It was then pickled in an acid bath to remove oxide scale caused by annealing and restore the corrosion resistance. After that, the material was roll leveled to improve the flatness.

The main measured mechanical properties perpendicular to the rolling direction at room temperature are yield strength $R_{P0.2}$ 230 MPa, ultimate tensile strength R_m 642 MPa, elongation 54%, and hardness 170 HB. The material was delivered in the form of test coupons with dimensions 400 × 150 × 2mm. An EBSD mapping showing the microstructure of the material is presented in Fig. 1. Around 1.7% of ferrite was present in the material, which is normal for 304L. The ferrite measurement was done according to ASTM E1245 after etching in

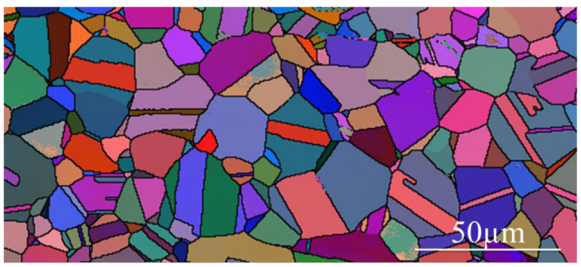

Fig. 1 Cross-section microstructure and grain orientation of 304L austenitic stainless steel in the as-received condition

40% NaOH solution, using 2.5 V for 3 s and was calculated over 10 fields at ×1000 magnification. The fields were chosen from one edge to the other, i.e., throughout the thickness. Less ferrite was seen close to the edge/surface, compared to the middle section/bulk.

Grinding operations

A Chevalier FSG-2A618 grinding machine was used for the grinding operations; the set-up is shown in Fig. 2. As shown in the figure, grinding belts (50 mm in width, 473 mm in length) with conventional aluminum oxide grits were mounted on the grinding wheel and test coupons (400 × 150 × 2mm) were fixed by screws on the edges to the working table during grinding. The grinding wheel (50 mm in width, 150 mm in diameter) used was from the Kemper Radix Go series, which is an expanding roller made of 20-mm-thick rubber. All grinding operations were conducted along the rolling direction of the material. A fixed grinding speed, $v_s = 23m/s$, and fixed feed rate, $v_w = 8m/\text{min}$, were used, based on the recommendation from the material supplier. During grinding, the grinding wheel rotated clockwise, and the working table was moved back and forth; thus, both up and down grinding were performed during the operation. The grinding parameters which were varied were

Fig. 2 Grinding set-up

the abrasive grit size, the machine power, and the grinding lubrication; these are also parameters that can be varied in an industrial grinding process to achieve different grinding results in addition to cutting speed and feed rate. The machine power means a certain percentage of the total motor power, which is 1 kW, is used to drive the grinding belt around. During grinding, a given machine power was used, and the grinding force was adjusted manually by a hand wheel to reach the given machine power. The grinding lubrication used was 3% of Mobilcut 321, which is a synthetic fluid with specific gravity of 1.10 at 20 °C and a pH value of 9.4. During grinding, the lubrication was poured onto the workpiece surface, and the path of the lubrication has been described in detail in a previous paper (Zhou, Peng Ling, et al. 2016).

Three groups of ground samples were prepared to investigate the influence of three grinding parameters, including (I) abrasive grit size, (II) machine power, and (III) grinding lubrication. The detailed grinding parameters and procedures given in Table 1 were selected based on recommendations by the material supplier. Grinding started with a coarse grit (60#) for 5 min to remove the original surface. Further grinding was carried out in steps with finer grit in each step until the desired surface finish had been reached (Outokumpu 2013). For each step, a new abrasive was used and grinding was performed long enough to remove the deformation induced from the previous step.

For the investigation of the influence of the abrasive grit size, 60# (165~405 μm), 180# (25~114 μm), and 400# (11~45 μm) grits were used as the final surface finish, respectively. In this case, 60% machine power was maintained and no grinding lubrication was used. To investigate the machine power effect, the same grit size (180#) was used as the final surface finish and no lubrication was employed. The machine power used was 30%, 60%, or 90%. The study of lubrication influence was performed by grinding with and without lubrication while keeping the final surface finish (180#) and machine power (60%) the same. In order to avoid too large a test matrix, and since grinding without lubricant is more interesting from the perspective of both production cost and environmental issues, the effect of grinding lubrication was restricted to only one condition.

Characterization methods

Since the grinding force was adjusted by the machine power, a piezo-electric transducer-based dynamometer (Kistler 7257B) was mounted under the working table to measure the normal force during grinding operations, as shown in Fig. 2. The Kistler 7257B was connected to a PC using a National Instruments data acquisition device. The measured force values were read manually. Due to

Table 1 Grinding parameters and procedures for each sample

Group no.	Comparison	Grit size	Machine power	Lubrication	Grinding procedures
I	Abrasive grit size	60#	60%	Without	60#(5 min) + 60#(2.5 min)
		180#			60#(5 min) + 180#(5 min)
		400#			60#(5 min) + 180#(5 min) + 280#(5 min) + 400#(5 min)
II	Machine power	180#	30%	Without	60#(5 min) + 180#(5 min)
			60%		
			90%		
III	Lubrication	180#	60%	Without	60#(5 min) + 180#(5 min)
				With	60#(lubrication 5 min) + 180#(lubrication 5 min)

vibrations in the grinding table, the planar forces were difficult to measure accurately. Thus, in the current paper, the measured force is the force acting perpendicularly on the contact zone of grinding and is termed the normal grinding force. A FLIR i5 infrared camera was used to measure the ground surface temperature during operation. The emissivity setting of the camera was 0.95; the measured spots were near the contact area between the workpiece material and the grinding wheel.

A square sample of 30 mm in edge length was taken from as-delivered plate and each ground plate to check the plate thickness, and thus investigate the metal removal by different grinding conditions. Using a Mitutoyo digital indicator (1 μm resolution) mounted on a Mitutoyo granite plate; thicknesses at the four corners of the sample were measured manually. For each corner, 6 repeat measurements were made, i.e. 24 thickness values, and the mean value was taken as the thickness of the plate.

A 3D optical topometer (Wyko NT9100) was used to measure the surface roughness, choosing five points (1.3×0.95 mm in area) for each ground sample, and then averaging. To investigate the surface topography and surface defects, a scanning electron microscopy (SEM, FEG-SEM Zeiss Ultra 55) was used in this study.

Electron channeling contrast imaging (ECCI) is a technique that can provide diffraction contrast images to analyze deformation, damage, strain field, or even individual defects in crystalline materials (Johansson et al. 2013). In this study, a Hitachi FEG-SEM SU-70 was used to study the cross-section microstructural development by different grinding operations.

The residual stresses in the surface layer parallel ($\sigma_{\parallel}$) and perpendicular ($\sigma_{\perp}$) to the grinding direction were determined by X-ray diffraction. Cr-K_a radiation was used, giving a diffraction peak at 2θ~128° for the {220} lattice planes of the austenitic phase. Peaks were measured at nine ψ-angles (ψ = ±55°, ±35°, ±25, ±15°, 0°). The Pseud-Voigt profile (Hauk 1997) was used to determine simultaneously peak positions and peak width in full width at half maximum (FWHM) for both the K_{a1} and K_{a2} diffraction peaks, and the results presented in this study are from the K_{a1} diffraction peaks. Residual stresses were calculated based on the $\sin^2\psi$ method (Hauk 1997; Noyan and Cohen 1987) with an X-ray elastic constant of $6 \times 10^{-6} MPa^{-1}$. Controlled electrolytic polishing of an area of 12 mm in RD direction and 15 mm along the TD direction was used on one sample to remove the surface layer in order to measure the residual stresses in the sub-surface layer. No correction has been made for possible stress relaxation due to polishing.

Results and discussion

Grinding force and measured surface temperature

The effects of the grinding parameters on the grinding force and the measured surface temperature are compared in Table 2. The results show that increasing the machine power increases the required normal grinding force. The application of grinding lubrication was observed to reduce the normal grinding force from 100 to 40 N even though the same machine power (60%) was used. A similar effect has also been observed in previous work by the current authors when grinding duplex stainless steel 2304 (Zhou, Peng Ling, et al. 2016). Using lubrication during grinding operations can help to retain abrasive grit sharpness, reduce friction between abrasive and workpiece material, and contribute to a favorable mode of chip forming, thus reducing the normal force (Paul and Chattopadhyay 1996).

As illustrated in Fig. 3, the surface temperatures were measured close to the contact area between the workpiece material and the grinding wheel. Since it is the temperature in the grinding zone that actually affects the ground surface properties and the measured temperature values are influenced by the surface conditions as well as the settings of the infrared camera, the results given here are used only to indicate the tendency of the temperature change for different grinding parameters. Grinding with a higher machine power significantly increased the surface temperature. The increase of machine power directly increased the grinding force and the resulted

Table 2 Measured grinding force and surface temperature by different grinding conditions

Group no.	Comparison	Grinding parameters			Measured normal grinding force (±10 N)	Measured surface temperature
		Final surface finish	Machine power	Lubrication		
I	Abrasive grit size	60#	60%	Without	100 N	60 °C
		180#			100 N	68 °C
		400#			100 N	70 °C
II	Machine power	180#	30%	Without	60 N	50 °C
			60%		100 N	68 °C
			90%		150 N	85 °C
III	Lubrication	180#	60%	Without	100 N	68 °C
				With	40 N	35 °C

higher friction between the abrasive and workpiece material caused an obvious increase in grinding heat. Somewhat counterintuitively, it was seen that grinding with finer final surface (group I) resulted in slightly higher surface temperatures. The most plausible explanation for this is that a finer finish added more steps of grinding procedures and increased the total grinding time. Because heat generated by each grinding step was accumulated, a slight increase in the surface temperature was observed. However, the machine power has a much bigger influence on temperature. The cooling effect with lubrication is notable although the temperature measured in the lubrication condition may possibly be that of the lubricant rather than the metal surface; lubrication can effectively reduce friction between the abrasive grits and the workpiece, and help remove grinding heat (Yao et al. 2013). In general, the measured grinding surface temperature close to the grinding zone is relatively low in this study.

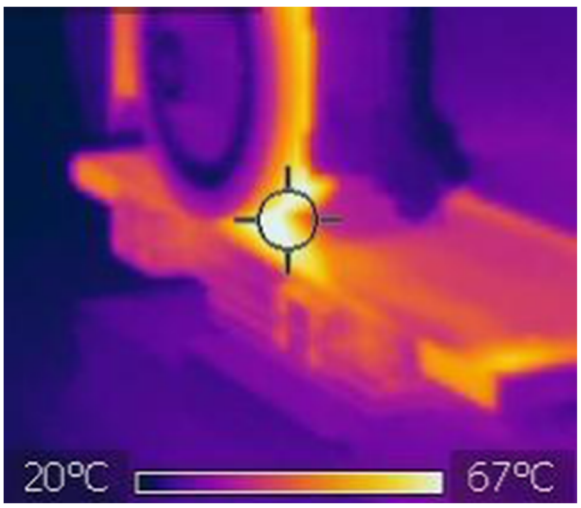

Fig. 3 Temperature measurement during grinding operations, showing the measured area, 304L ground by 180# abrasive grit size, 60% machine power, and without using grinding lubrication

Metal removal

Calculated metal removal results in different grinding conditions as well as standard errors are shown in Fig. 4. The metal removal is calculated according to the following equation:

$$\delta_{\text{metal removal}} = \delta_{\text{as delivered material}} - \delta_{\text{after grinding operation}} \quad (1)$$

where $\delta_{\text{metal removal}}$ is the thickness of metal removal due to different grinding operations

$\delta_{\text{as delivered material}}$ is the thickness of as delivered test coupon$\delta_{\text{after grinding operation}}$ is the thickness of test coupons after different grinding operations

Here, the thickness of the test coupons, both in the as-delivered and ground states, is the mean value of the 24 measured thickness values for each plate; the estimated standard errors of random intercept are calculated by the mixed effect model (Cheng 2014), they can be interpreted as production errors, which are only associated with plate thickness variation, the error from the reproducibility was excluded.

As shown from Fig. 4a, both 60# and 180# grit size abrasives have good metal removal ability. 28 μm of metal was ground away by using a 60# grit size abrasive; and 20 μm more in thickness was removed by adding one more step of the grinding process using the 180# grit size abrasive. However, the 280# and 400# grit size abrasives have relatively lower metal removal ability, they are used for the surface finish process; only 8 μm in thickness of metal was ground away by using a 280# grit size abrasive for 5 min plus another 5 min grinding by a 400# grit size abrasive. The machine power also has a large influence on the metal removal behavior. As illustrated in Fig. 4b, when using same grit size abrasives and same grinding procedures, a maximum metal removal rate was seen with the intermediate power (60%). A lower machine power (30%) gave 25 μm of metal removal compared to 48 μm at 60%, at 90% power the

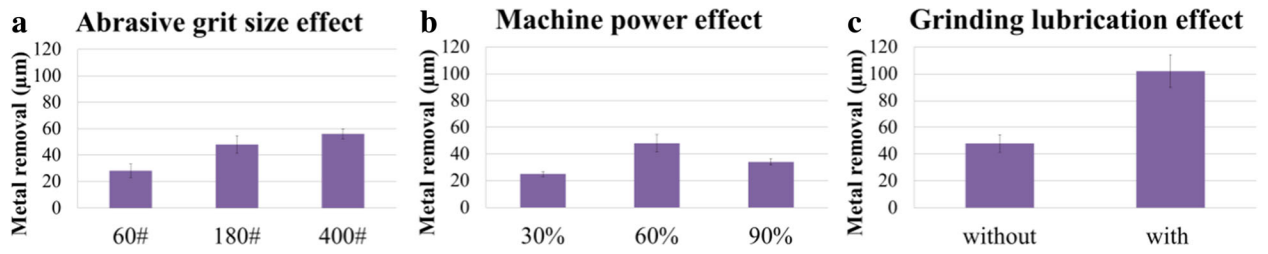

Fig. 4 Comparison of metal removal by different grinding conditions. **a** Group I, abrasive grit size effect. **b** Group II, machine power effect. **c** Group III, grinding lubrication effect

metal removal dropped to 34 μm. Higher machine power introduced higher grinding force. When grinding with a lower machine power (grinding force), the abrasive grits slide and rub over the material surface instead of effective cutting and ploughing. Using a higher machine power (grinding force) increased friction between the abrasive and the workpiece surface as well as wear of abrasive grits. Figure 4c shows the significant improvement of metal removal ability by using grinding lubrication; the removed thickness was more than doubled (from 48 μm increased to 102 μm) by using lubricant. This can be explained by the fact that grinding lubrication can help reducing friction at the contact surfaces, diffusing away heat, retaining sharpness of the abrasive grits, thus induces a favorable metal removal mode (Manimaran et al. 2014; Fredj et al. 2006).

Ground surface roughness and topography

In this study, surface roughness was measured using both R_a and R_z values. Figure 5 gives the results for different abrasive grit size (group I), error bars in the figure are standard deviations calculated from the five measurements for each sample. As shown from the figure, both R_a and R_z values are decreased by using a finer grit size abrasive as the final surface finish. For the coarse (60#) abrasive grit size, a R_a value of 1.81 μm and a R_z value of 18.4 μm were measured. With a finer (180#) grit size, both R_a and R_z values were reduced to around the half (R_a = 0.77 μm and R_z = 10.66 μm), while for the finest (400#) grit size, the R_a value decreased to 0.34 μm and R_z to 5.66 μm.

Figure 6 presents SEM images showing the surface topography and surface defects resulting from using different abrasive grit size (group I). Deep grooving, smearing, adhesive chips, and indentations, shown in Fig. 6a, are the main defects observed on the ground surfaces. Similar defects have also been observed when grinding duplex stainless steel 2304 in the authors' previous work (Zhou, Peng Ling, et al. 2016). The formation of such defects is related to different interactions between the grinding grits and workpiece surfaces. The non-uniform metal removal process, including chip forming and ploughing, introduced deep grooves on the ground surfaces. At the contact zone between the abrasive grit tops and the workpiece surface, material is pushed out and moved across the surface, leading to smearing areas (Totten et al. 2002) in addition to chip formation. The redeposition process (Turley and Doyle 1975) caused adhesive chips; the material was transferred to the grits by adhesion, and then was transferred back to the ground surface by friction welding. Rubbing contact between abrasive grits or cut down chips and workpiece surface caused formation of indentations. As shown from the figure, the surface finish was clearly improved by using finer grit size abrasives. Compared with using 60# grit size abrasive, it was clear that deep grooves, large smearing areas, and adhesive chips were reduced by using a 180# grit size abrasive. Surface defects were reduced even more by using the finest (400#) grit size. For all three samples, surface indentations have been observed.

The abrasive grit size has a major influence on the surface roughness and the surface finish, the improvement by using a smaller grit size abrasive is significant. During grinding, only a small top region of the abrasive grits is

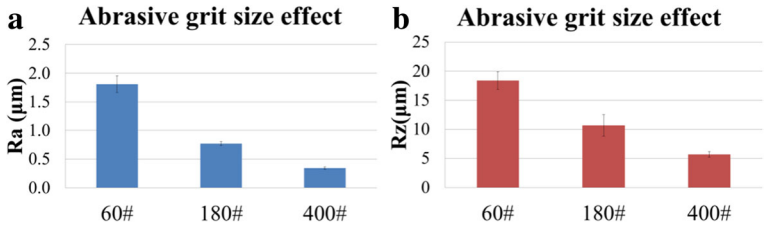

Fig. 5 Surface roughness by different abrasive grit size (group I). **a** R_a factor. **b** R_z factor

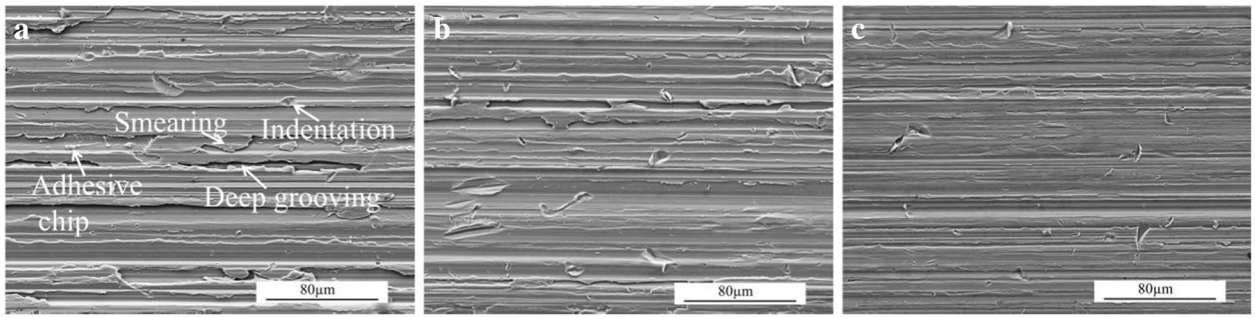

Fig. 6 Surface topography and surface defects by different abrasive grit size (group I). **a** 60#. **b** 180#. **c** 400#

efficient for metal removal, the remaining part is sliding and rubbing the workpiece material (Sin et al. 1979). The coarser grit size abrasives have bigger abrasive particles, causing larger areas of rubbing during grinding; meanwhile, the size and distribution of the abrasive grit grains are more uneven in coarser grit size abrasives; thus, more defects and a worse surface finish have been induced by using coarser grit size abrasives.

Figures 7 and 8 illustrate the effect of machine power (group II) on the ground surface roughness and surface topography, respectively. Compared with grinding by different grit size abrasives, the machine power has a much smaller influence on ground surface roughness. The R_a values shown in Fig. 7 varied very little although the machine power has been doubled and tripled while the R_z values show some variation. The effects on surface topography and surface defects are different; the SEM images (Fig. 8) show a clear improvement of surface finish by increasing the machine power. The ground surface appeared much smoother, with fewer surface defects when the machine power was increased to 90% (Fig. 8c), although many small smearing areas were still observed. Stainless steel 304L has high toughness and high ductility (Outokumpu 2013), and has been characterized as 'gummy', i.e., rubbery, or adhesive, during machining (Jang et al. 1996). A lower machine power means a lower (normal) grinding force, which led to more rubbing instead of the effective metal removal processes chip forming, cutting, or ploughing, as demonstrated by the results in Fig. 4. Together with the high adhesion of the material on the grinding belt, large smearing areas as well as adhesive chips were generated. Meanwhile, a higher machine power means a higher downward force, therefore, instead of being cut, surface material was pressed down and slid along the grinding direction. As a result, a higher degree of strain hardening with the ground surface reduced the rubbery or adhesive behavior and improved surface finish after grinding, although a large amount of smearing areas remained. However, it should be noted that the effect of varying machine power also depends on the property of workpiece material. For example, in Zhou, et al.'s work (Zhou, Peng Ling, et al. 2016) on grinding of duplex stainless steel 2304, there is an optimum machine power for grinding, above and below which the surface finish becomes poorer.

Figures 9 and 10 present the influence of grinding with and without lubrication (group III) on surface roughness and surface topography, respectively. By using lubrication during grinding operations, large improvements of the surface roughness and surface finish are achieved, as seen in the figures. Both R_a and R_z values decreased to nearly a half, while the reduction of ground surface defects is very evident. This can be explained by decreased friction with good lubrication, which in turn retained abrasive sharpness and enhanced more uniform effective metal removal. Meanwhile, the reduction of surface temperature during grinding with lubrication also reduced the material's rubbery or adhesive behavior and it reduced redeposition.

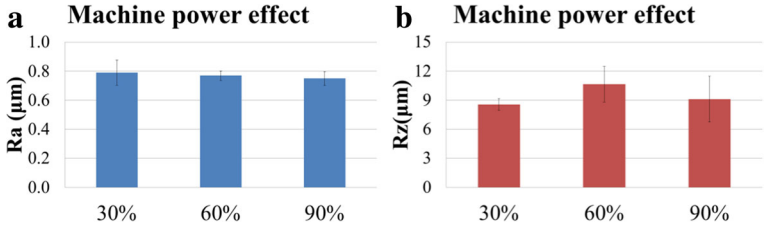

Fig. 7 Surface roughness by different machine power (group II). **a** R_a factor. **b** R_z factor

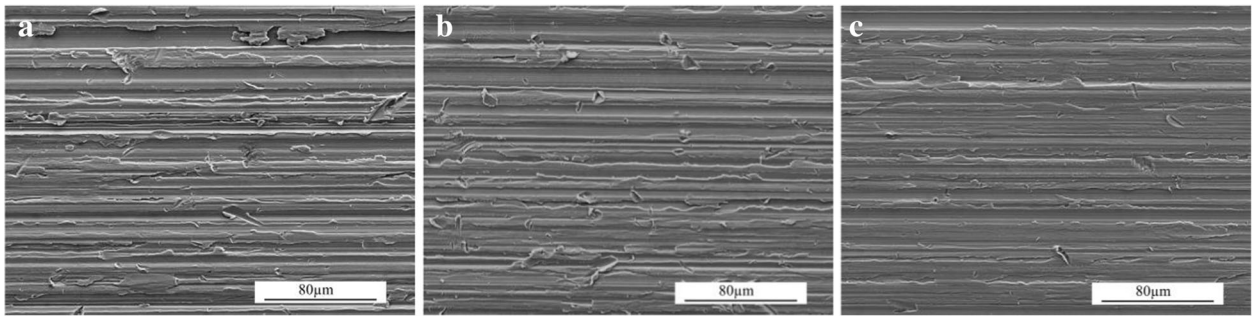

Fig. 8 Surface topography and surface defects by different machine power (group II). **a** 30%. **b** 60%. **c** 90%

Cross-section microstructure

Backscattered electron microscopy images revealing typical cross-section microstructures near the grinding surfaces when using different grit size abrasives (group I), different machine powers (group II), and wet/dry grinding (group III) are shown in Figs. 11, 12, and 13, respectively. Various magnifications have been used to investigate the microstructural development. For all the presented images, the grinding direction is perpendicular to the sample's cross-section. Similar features were observed for all the ground samples, which are illustrated in Fig. 11a1, a2. Depending on the grinding parameters used, smearing of different size and amount, adhesive chips, or cold welded chips with an irresolvable microstructure was observed along the ground surfaces. A heavily deformed surface layer extending up to a few microns from the ground surface was formed, followed by a much thicker sub-surface layer showing less plastic deformation. The heavily deformed surface layer comprised fragmented grains and dislocation sub-cells. Such a surface layer has also been observed in other ground materials, for example, in ground duplex stainless steel 2304 in work by the current authors (Zhou, Peng Ling, et al. 2016). The sub-surface region is characterized by slip bands and strain contrast (different grey shades) from plastic deformation. Next to the surface layer, densely populated and deformed slip bands of multiple orientations were observed, while further away slip bands became fewer and straighter as the degree of plastic deformation decreased. For all the investigated samples, the grinding induced deformation zone was much smaller than the abrasive grit size used.

Corresponding to the surface topography observations, a high amount of large smearing areas or adhesive chips (Fig. 11a1) was observed in the cross section from grinding by using 60# grit size abrasive. In addition, cold welded chips with formation of microcracks (Fig. 11a2) were also visible. Both the amount and size of such defects decreased when finer (180# and 400#) grit size abrasives were used. Images in Fig. 11 show that the abrasive grit size has major influence on both the degree of deformation and the deformation depth. Grinding with a 60# grit size abrasive induced a heavily deformed surface layer of 3–4 μm in thickness with a clear fragmented grain structure. The thickness of the heavily deformed layer was reduced to nearly the half when using 180#, and around one third by 400#. Meanwhile, coarse abrasive grit (60#) induced a deformed sub-surface layer of over 20 μm in thickness. The thickness of the deformation-affected layer reduced between 15 and 10 μm when using 180# and 400# abrasive grit sizes, respectively. Both the density of slip bands and the number of deformation slip systems was reduced by using finer grit size abrasives, which again indicated smaller deformation.

The low machine power (30%) induced a large amount of small smearing areas or adhesive chips along the grinding surface, which agrees with the results from the surface topography investigation, while very few cold welded chips resulted. As shown before, the normal grinding force was low. As a result, metal removal became less effective; abrasive grits slid over the material surface, introducing many smearing areas as well as

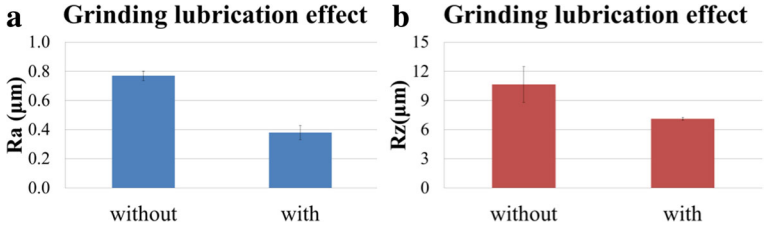

Fig. 9 Surface roughness with/without using grinding lubrication (group III). **a** R_a factor. **b** R_z factor

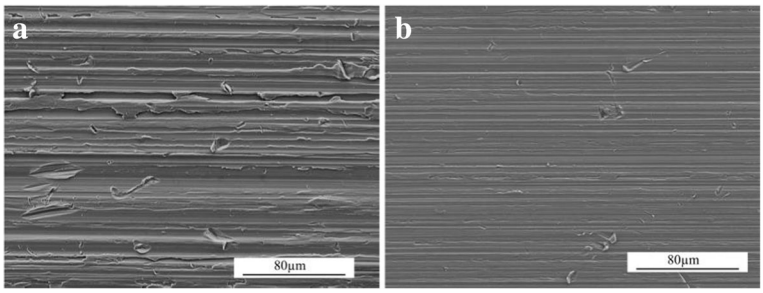

Fig. 10 Surface topography and surface defects (**a**) without and (**b**) with using grinding lubrication (group III)

adhesive chips on the ground surface. On the other hand, as the friction between the abrasive and workpiece material was low, the grinding temperature was low and thus few cold welding chips could form. In the case of grinding at 90% machine power, more grinding heat was generated due to increased grinding friction and promoted the formation of cold welding chips. As shown in Fig. 12, which presents typical cross-section microstructures for different machining powers, the thicknesses of the highly deformed surface layers are similar. In the sub-surface region, the formation of slip bands indicated that the deformation intensity and deformation depth are also similar. However, deformation was found to be very non-uniform when grinding using 30% machining power. As illustrated in Fig. 12a1, a2, which are from the same sample, some surface areas were highly deformed while in others the deformation was very small.

Using grinding lubrication largely reduced the formation of smearing, adhesive chips, and cold welded chips on the ground surface, which can be simply explained by the measured lower normal grinding force and lower temperature. From the electron channeling images presented in Fig. 13, the reduction of deformation is also obvious; although the thickness of the deformed surface layer is similar, the deformation in the sub-surface region is much lower. As shown in Fig. 13b, continuous deformation fringes were observed with a few slip bands formed only in a range of several microns. Meanwhile,

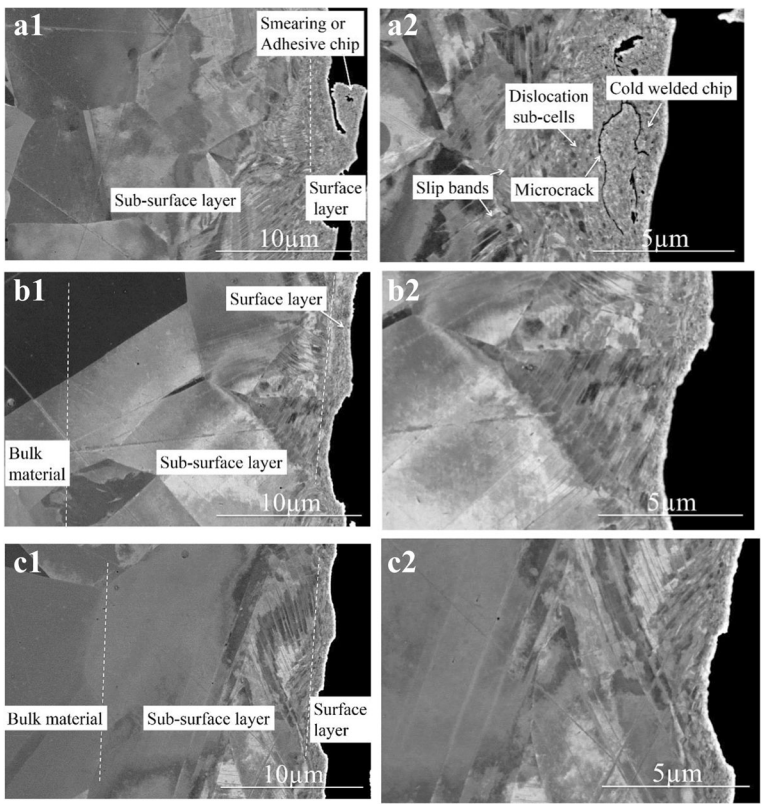

Fig. 11 Cross-section microstructure after using different abrasive grit size (group I). **a** 60#. **b** 180#. **c** 400#

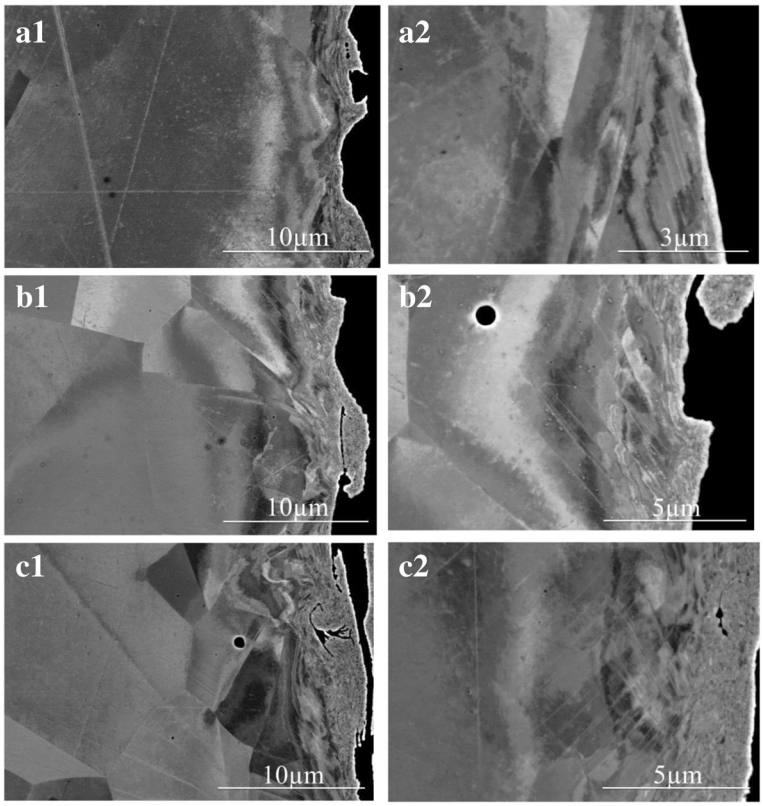

Fig. 12 Cross-section microstructure resulting from use of different machine power (group II). **a** 30%. **b** 60%. **c** 90%

deformation was found to be more uniform by using grinding lubrication.

Ground surface residual stresses

The full width at half maximum method (FWHM) reveals the broadening of a diffraction peak, which can be related to an increased density of crystal defects in a material (Chen et al. 2014). Here the observed difference in FWHM is considered to be related to different surface deformations from the grinding processes. In Fig. 14, diffraction peaks measured on the as-delivered surface and on the ground surface by 180# abrasive grit size,

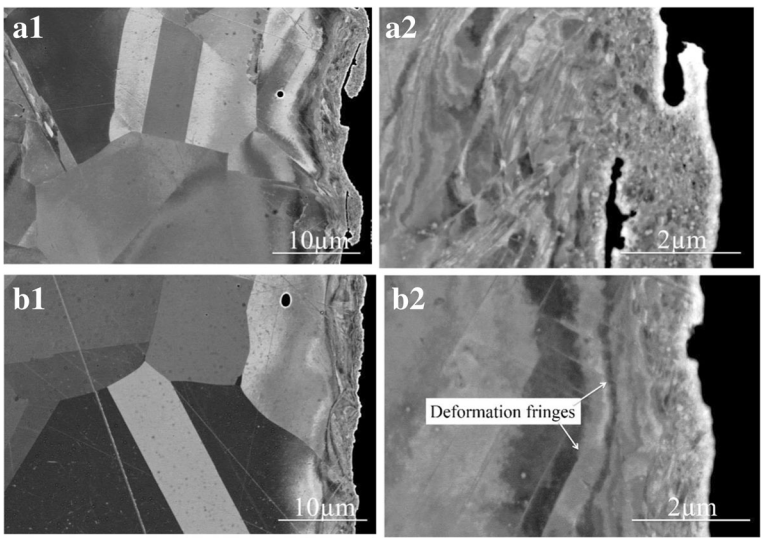

Fig. 13 Cross-section microstructure (**a**) without and (**b**) with grinding lubrication (group III)

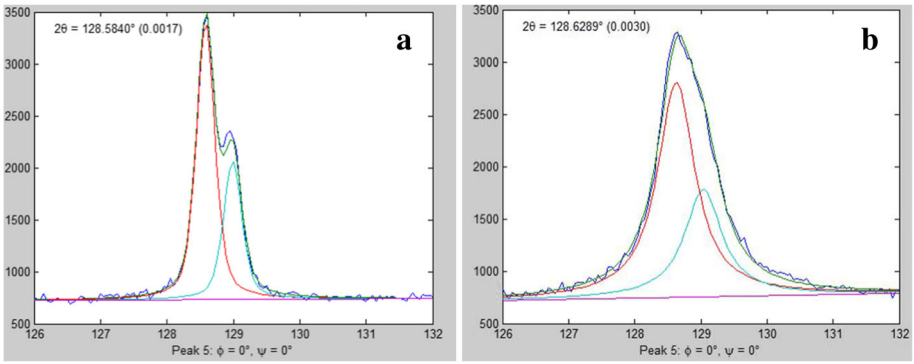

Fig. 14 Diffraction peaks measured (*in black*) from (**a**) as-delivered surface, (**b**) ground surface by 180# abrasive grit size, 60% machine power and without using lubrication. The fitted peaks are also shown in *blue* with *red* for the $K_{\alpha 1}$ *and light blue* for the $K_{\alpha 2}$ *peaks*

60% machine power, without using lubrication are illustrated respectively. The FHWM of the $K_{\alpha 1}$ peak is 0.332° for the as-delivered surface and 0.68° for the ground surface. The FWHM results of all ground surfaces by different grinding parameters as well as the as-delivered material are presented and compared in Fig. 15. A lower FWHM by using finer grit size abrasives or grinding lubrication was observed (Fig. 15a and c), indicating smaller surface deformation induced by these grinding operations. On the other hand, as illustrated in Fig. 15b, the influence of the machine power on the surface deformation is relatively small while the influence from the abrasive grit size is more dominant. The FWHM results agree with the observed microstructural changes in the ground surface.

The surface residual stresses parallel ($\sigma_{\parallel}$) and perpendicular ($\sigma_{\perp}$) to the grinding directions by different grinding conditions are presented in Fig. 16. Uncertainties of the obtained residual stresses, given as error bars in the figures, are derived from standard deviations in diffraction peak fitting as well as for deviations of the measured diffraction peak positions from expected distributions with measurement directions according to the elastic theory for a quasi-isotropic material.

As shown from the figure, the grinding operations in this study generated tensile $\sigma_{\parallel}$ and compressive $\sigma_{\perp}$ stresses in the ground surfaces. The highest surface tensile residual stress, up to 374 ± 44 MPa, was induced by using the coarse (60#) grit size abrasive, as seen in Fig. 16a. The tensile $\sigma_{\parallel}$ was reduced nearly by one third, to 228 ± 25 MPa, by using a finer (180#) grit size abrasive, while the compressive $\sigma_{\perp}$ stress was similar. However, when using the even finer (400#) grit size abrasive, the surface tensile $\sigma_{\parallel}$ stress increases but the compressive $\sigma_{\perp}$ stress decreases. The trend of the machine power influence on surface residual stresses is very clear from Fig. 16b ,i.e., higher machining power generated a higher tensile $\sigma_{\parallel}$ stress but lower compressive $\sigma_{\perp}$ stress in the ground surfaces. The effect of using grinding lubrication is also obvious, as shown in Fig. 16c: using grinding lubrication reduced residual stresses, both $\sigma_{\parallel}$ and $\sigma_{\perp}$, in the surface layer.

For the sample ground with 60# grit size abrasive, the in-depth residual stress profile parallel ($\sigma_{\parallel}$) and perpendicular ($\sigma_{\perp}$) to the grinding direction as well as the FWHM profile were also measured. As shown in Fig. 17, the grinding induced tensile $\sigma_{\parallel}$ stress decreased dramatically from 374 to 44 MPa at the surface to compression within a depth of around 15 μm beneath the ground surface. The compressive $\sigma_{\perp}$ stress increased from 91.1 to 18 MPa at the surface to over 200 MPa in the subsurface region and then dropped gradually to zero in the

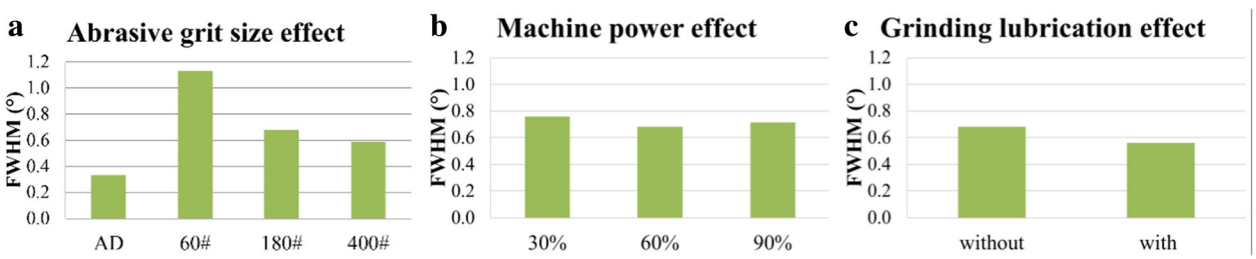

Fig. 15 Full width at half maximum after different grinding conditions. **a** Group I, abrasive grit size effect. **b** Group II, machine power effect. **c** Group III, grinding lubrication effect

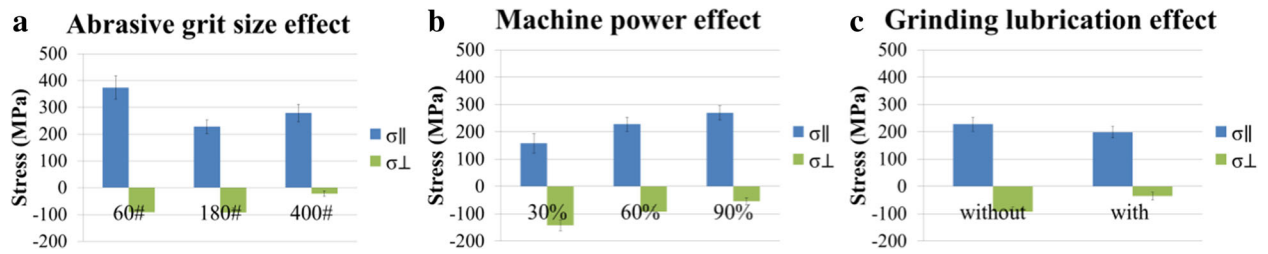

Fig. 16 Surface residual stresses induced by different grinding conditions. **a** Group I, abrasive grit size effect. **b** Group II, machine power effect. **c** Group III, grinding lubrication effect. Positive stresses are tensile and negative stresses are compressive

bulk material. The results indicated the trend that residual stresses both along and transverse to the grinding direction largely shifted towards compression under the ground surfaces. High tensile residual stresses exist only in a very thin surface layer along the grinding direction. Such large residual stress gradients in the near surface region are typical for machined workpieces (Zhou, Peng Ling, et al. 2016). Meanwhile, a decrease of FWHM with increasing depth was also observed and reveals plastic deformation gradient under the ground surface.

During grinding, mechanically and thermally induced residual stresses are predominant and they exist simultaneously (Davim 2010). The mechanical interactions between the abrasive and the workpiece material tend to cause anisotropic residual stresses in the ground surface. The surface layer of the workpiece material parallel to the grinding direction experiences compressive plastic deformation; while perpendicular to the grinding direction, tensile deformation dominates (Guo et al. 2010; Noyan and Cohen 1987). As a result, the interaction between the surface layer and the bulk material leaves the ground surface in a condition of tension along the grinding direction but compression in the transverse direction. This is also seen in the present work.

Heat was generated in the contact zone between the abrasive and the workpiece material during grinding

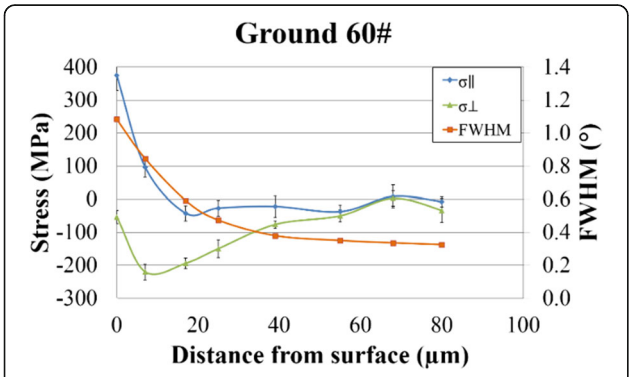

Fig. 17 In-depth residual stresses and full width at half maximum profiles after grinding by 60# as final surface finish (Zhou, Pettersson, et al. 2016)

operations, because of the low thermal conductivity of the stainless steel 304L, a temperature gradient was formed from the surface to the bulk material. This results in tensile stresses in both the directions during the cooling period after the grinding zone moved away (Fredj et al. 2006; Davim 2010). In this study, the measured highly anisotropic nature of the surface residual stress field, as well as the relatively low surface temperature in all of the ground samples, indicates that mechanically induced residual stresses dominate over thermally induced residual stresses.

When grinding with a 60# grit size abrasive, the high surface plastic deformation as well as grinding heat induced a high tensile ($\sigma_{\parallel}$) stress, which was reduced by using the 180# grit size abrasive because of the lower mechanical effect. However, compared with the 180#, the use of the 400# grit size abrasive generated more tensile residual stresses, both ($\sigma_{\parallel}$) and $\sigma_{\perp}$. This is probably attributable to the larger number of grinding steps when grinding with finer (280# and 400#) grit size abrasives, which introduces more accumulated heat on the surface, thus the increased thermal effect plus the decreased mechanical effect led to higher tensile residual stresses in the surface. The trend of the surface residual stresses with different machining powers is very obvious. A higher machining power increased the grinding temperature; but both the microstructure investigation and the FWHM results showed that the deformation of the surface and the sub-surface layer are similar at different used machining powers. Thus, an increasing thermal effect can be considered as the main factor that introduces higher tensile residual stresses, both parallel and perpendicular to the grinding directions when grinding at a higher machining power. Using grinding lubrication decreased both surface deformations and heat from the grinding operation; however, the decreased surface tensile ($\sigma_{\parallel}$) stress and compressive $\sigma_{\perp}$ stress results indicate that the reduction of mechanical effects was more significant than that of the thermal effects in this study.

Conclusions

The effect of different grinding parameters on the processing and the surface properties of the austenitic

stainless steel 304L has been investigated. The following conclusions can be drawn:

- A higher machining power results in a larger normal grinding force; while using grinding lubrication reduces the normal force.
- A higher machining power increases the grinding temperature, while the grinding lubrication has an effective cooling effect. A slight increase in temperature with finer grit sizes was attributed to the cumulative effect of a longer total grinding time.
- A coarser grit size abrasive gives a higher metal removal ability, and lubrication significantly increases the metal removal rate. For the investigated 304L austenitic stainless steel, there is an optimum machining power for the effective removal of material.
- Using smaller grit size abrasives or grinding lubrication results in fewer surface defects. Although the influence of the machining power on the surface roughness was small, a higher machining power was seen to improve the surface finish of austenitic stainless steel 304L.
- Cross-section microstructure investigations indicate that a coarser grit size, a higher machining power and grinding without lubrication introduce higher plastic deformation in the ground surface. A low machine power causes a non-uniform deformation zone while grinding lubrication gave a more uniform deformation zone. Microcracks were observed along the ground surface for all samples; although the number and size vary with the grinding parameters. These microcracks may be liable to initiate crevice corrosion.
- The grinding operation induces anisotropic residual stresses in the surface layer, with a tensile stress parallel and a compressive stress perpendicular to the grinding direction. The residual stress level depends on the grinding conditions. Residual stresses both along and transverse to the grinding direction are largely shifted towards compression in the sub-surface layer. The high tensile residual stresses generated parallel to the grinding direction are likely to affect the material's susceptibility to stress corrosion cracking. The measured residual stress anisotropy and the observed relatively low grinding surface temperature indicate that mechanical effect dominated over thermal effects in this study. It is suggested that the grinding direction could be optimized to give compressive stresses in the direction of the highest applied load and thus reduce the risk for stress corrosion cracking.

Acknowledgements
The authors are grateful to Outokumpu Stainless Research Foundation, Region Dalarna, Region Gävleborg, Länsstyrelsen Gävleborg, Sandvikens kommun, Jernkontoret and Högskolan Dalarna for financial support. Professor Stefan Jonsson is acknowledged for his contribution to the initial plan of this work. The authors express our gratitude towards Mikael Schönning and Timo Pittulainen at Outokumpu Stainless AB for providing the test materials and material data. The assistance with part of the sample preparation work by Annethe Billenius is also appreciated.

Authors' contributions
All the authors contributed to the design of the work. NZ contributed to the major part of the experiments, evaluation and writing. RLP ran part of the XRD measurements and commented on the manuscript. RP revised the work critically. All authors read and approved the final manuscript.

Authors' information
Nian Zhou is a PhD student at the Material Science Department of Dalarna University and KTH (Royal Institute of Technology), Sweden. She works on the influence of grinding operations on surface integrity and chloride-induced stress corrosion cracking of stainless steels for her PhD project, and the project is sponsored by Outokumpu Stainless Research Foundation. She has published three papers for the PhD work and co-authored six papers for her master degree.
Ru Lin Peng is currently associate professor at Linköping University, Sweden. She received her PhD in Engineering Materials from Linköping University in 1992 and worked at the Studsvik Neutron Research Laboratory of Uppsala University before joining the Department of Management and Engineering of Linköping University as a faculty member in 1997. Peng's research concerns enhancing surface properties of engineering materials, and she has coauthored over 130 articles.
Rachel Pettersson is research manager at Jernkontoret (The Swedish Steel Producers' Association) and adjunct professor in Corrosion Science at KTH (Royal Institute of Technology). Formerly, she was department manager with Outokumpu Stainless and section manager at Swerea KIMAB. She has over 130 publications on pitting corrosion, stress corrosion cracking, high temperature corrosion, stainless steels.

Competing interests
The authors declare that they have no competing interests.

Author details
[1]Department of Material Science, Dalarna University, SE-79188 Falun, Sweden. [2]KTH, SE-10044 Stockholm, Sweden. [3]Department of Management and Engineering, Linköping University, SE-58183 Linköping, Sweden. [4]Jernkontoret, SE-11187 Stockholm, Sweden.

Received: 23 November 2016 Accepted: 31 January 2017
Published online: 20 February 2017

References

Acharyya, S., Khandelwal, A., Kain, V., Kumar, A., & Samajdar, I. (2012). Surface working of 304L stainless steel: impact on microstructure, electrochemical behavior and SCC resistance. *Materials Characterization, 72*, 68–76.
Boothroyd, G., & Knight, W. (2005). *Fundamentals of metal machining and machine tools*, 3 ed. CRC Press
Chen, Z., Peng, R., Avdovic, P., Moverare, J., Karlsson, F., Zhou, J., & Johansson, S. (2014). Analysis of thermal effect on residual stresses of broached Inconel 718. *Advanced Materials Research, 996*, 574–579.
Cheng, H. (2014). *Analysis of panel data*, 3 ed. Cambridge University Press
Davim, J. P. (2010). *Surface intergrity in machining*. Springer
Dieter, G. E. (1989). *Mechanical Metallurgy* (pp. 699-704). McGraw-Hill
Fredj, N. B., Sidhom, H., & Braham, C. (2006). Ground surface improvement of the austenitic stainless steel AISI 304 using cryogenic cooling. *Surface & Coatings Technology, 200*, 4846–4860.
Guo, G., Liu, Z., Cai, X., An, Q., & Chen, M. (2010). Investigation of surface integrity in conventional grinding of Ti-6Al-4V. *Advanced Materials Research, 126–128*, 899–904.
Hauk, V. (1997). *Structural and Residual Stress Analysis by Nondestructive Methods*. Elsevier Science

Jang, D., Watkins, T., Kozaczek, K., Hubbard, C., & Cavin, O. (1996). Surface residual stresses in machined austenitic stainless steel. *Wear, 194*, 168–173.
Jiang, L., Paro, J., Hänninen, H., Kauppinen, V., & Oraskari, R. (1996). Comparison of grindability of HIP austenitic 316L, duplex 2205 and Super duplex 2507 and as-cast 304 stainless steels using alumina wheels. *Journal of Materials Processing Technology, 62*, 1–9.
Johansson, S., Moverare, J., & Peng, R. (2013). Recent applications of scanning electron microscopy. *Practical Metallography, 50*, 810–820.
Kopac, J., & Krajnik, P. (2006). High-performance grinding - a review. *Journal of Materials Processing Technology, 175*, 278–284.
Manimaran, G., Pradeep Kumar, M., & Venkatasamy, R. (2014). Influence of cryogenic cooling on surface grinding of stainless steel 316. *Cryogenics, 59*, 76–83.
Noyan, I., & Cohen, J. (1987). *Residual Stress Measurement by Diffraction and Interpretation*. Springer
Outokumpu, (2013). Handbook of stainless steel.
Outwater, J., & Shaw, M. (1952). Surface temperature in grinding. *Transaction of the ASME, 74*, 73–86.
Paul, S., & Chattopadhyay, A. (1996). The effect of cryogenic cooling on grinding forces. *International Journal of Machine Tools and Manufacture, 36*, 63–72.
Poulain, T., Mendes, J., Henaff, G., & De Baglion, L. (2013). Influence of surface finish in fatigue design of nuclear power plant components. *Procedia Engineering, 6*, 233–239.
Sin, H., Saka, N., & Shu, N. (1979). Abrasive wear mechanisms and the grit size effect. *Wear, 55*, 163–190.
Totten, G., Howes, M., & Inoue, T. (2002). *Handbook of residual stress and deformation of steel*.
Turley, D., & Doyle, E. (1975). Factors affecting workpiece deformation during grinding. *Material Science and Engineering, 21*, 261–271.
Turnbull, A., Mingard, K., Lord, J., Roebuck, B., Tice, D., Mottershead, K., Fairweather, N., & Bradbury, A. (2011). Sensitivity of stress corrosion cracking of stainless steel to surface machining and grinding procedure. *Corrosion Science, 53*, 3398–3415.
Vashista, M., Kumar, S., Ghosh, A., & Paul, S. (2010). Surface integrity in grinding medium carbon steel with miniature electroplated monolayer cBN wheel. *Journal of Materials Engineering and Performance, 19*, 1248–1255.
Yao, C., Jin, Q., Huang, X., Wu, D., Ren, J., & Zhang, D. (2013). Research on surface integrity of grinding Inconel 718. *The International Journal of Advanced Manufacturing Technology, 65*, 1019–1030.
Zeng, Q., Liu, G., Liu, L., & Qin, Y. (2015). Investigation into grindability of a superalloy and effects of grinding parameters on its surface integrity. *Journal of Engineering Manufacture, 229*(2), 238–250.
Zhang, H., Chen, W., Fu, X., & Huang, L. (2012). Temperature measurement and burn mechanism of stainless steel 1Cr11Ni2W2MoV in grinding. *Materials Science Forum, 723*, 433–438.
Zhou, N., Peng Ling, R., & Pettersson, R. (2016). Surface integrity of 2304 duplex stainless steel after different grinding operations. *Journal of Materials Processing Technology, 229*, 294–304.
Zhou, N., Pettersson, R., Peng, R., & Schönning, M. (2016). Effect of Surface Grinding on Chloride Induced SCC of 304L. *Materials Science and Engineering A, 658*, 50–59.